
1 **Indirect contributions of global fires to surface ozone through**
2 **ozone-vegetation feedback**

3

4 **Yadong Lei^{1,2}, Xu Yue^{3*}, Hong Liao³, Lin Zhang⁴, Yang Yang³, Hao Zhou^{1,2},**
5 **Chenguang Tian^{1,2}, Cheng Gong^{2,5}, Yimian Ma^{1,2}, Lan Gao^{1,2}, Yang Cao^{1,2}**

6 ¹Climate Change Research Center, Institute of Atmospheric Physics, Chinese
7 Academy of Sciences, Beijing, 100029, China

8 ²University of Chinese Academy of Sciences, Beijing, 100029, China

9 ³Jiangsu Key Laboratory of Atmospheric Environment Monitoring and Pollution
10 Control, Collaborative Innovation Center of Atmospheric Environment and
11 Equipment Technology, School of Environmental Science and Engineering, Nanjing
12 University of Information Science & Technology (NUIST), Nanjing, 210044, China

13 ⁴Laboratory for Climate and Ocean–Atmosphere Studies, Department of Atmospheric
14 and Oceanic Sciences, School of Physics, Peking University, Beijing, 100871, China

15 ⁵State Key Laboratory of Atmospheric Boundary Layer Physics and Atmospheric
16 Chemistry (LAPC), Institute of Atmospheric Physics, Chinese Academy of Sciences,
17 Beijing, 100029, China

18 *Correspondence to:* Xu Yue (yuexu@nuist.edu.cn)

19

20

21

22

23 **Abstract:** Fire is an important source of ozone (O₃) precursors. The formation of
24 surface O₃ can cause damages to vegetation and reduce stomatal conductance. Such
25 processes can feed back to inhibit dry deposition and indirectly enhance surface O₃.
26 Here, we apply a fully coupled chemistry-vegetation model to estimate the indirect
27 contributions of global fires to surface O₃ through O₃-vegetation feedback during
28 2005-2012. Fire emissions directly increase the global annual mean O₃ by 1.2 ppbv
29 (5.0%) with a maximum of 5.9 ppbv (24.4%) averaged over central Africa by emitting
30 substantial number of precursors. Considering O₃-vegetation feedback, fires
31 additionally increase surface O₃ by 0.5 ppbv averaged over the Amazon in October,
32 0.3 ppbv averaged over southern Asia in April, and 0.2 ppbv averaged over central
33 Africa in April. During extreme O₃-vegetation interactions, such feedback can rise
34 to >0.6 ppbv in these fire-prone areas. Moreover, large ratios of indirect-to-direct fire
35 O₃ are found in eastern China (3.7%) and the eastern U.S. (2.0%), where the high
36 ambient O₃ causes strong O₃-vegetation interactions. With likelihood of increasing
37 fire risks in a warming climate, fires may promote surface O₃ through both direct
38 emissions and indirect chemistry-vegetation feedbacks. Such indirect enhancement
39 will cause additional threats to public health and ecosystem productivity.

40

41 **Keywords:** fires, surface ozone, dry deposition, ozone-vegetation feedback, GC-YIBs

42

43

44

Deleted: surface

Deleted:), which causes damage

Deleted: reduces

Deleted: mean

49 1 Introduction

50 Tropospheric ozone (O₃) is a toxic air pollutant with detrimental effects on vegetation
51 (Yue and Unger, 2014; Jurán et al., 2021). Plant stomatal uptake of O₃ decreases both
52 chlorophyll and Rubisco contents and increases the deformity rate of chloroplasts
53 (Booker et al., 2007; Akhtar et al., 2010; Inada et al., 2012), which further reduces the
54 leaf area index (LAI) and gross primary productivity (GPP) of ecosystems (Karnosky
55 et al., 2007; Ainsworth et al., 2012). Modeling studies estimated that O₃ damage
56 reduces global GPP by 1.5%-3.6% with regional maximum reductions of 8%-20%
57 over eastern U.S., western Europe, and eastern China (Yue and Unger, 2014; Lei et al.,
58 2020; Zhu et al., 2021). In turn, vegetation damage also influences both the sources
59 and sinks of O₃ through biogeochemical and biogeophysical feedbacks (Curci et al.,
60 2009; Heald and Geddes, 2016; Fitzky et al., 2019). The damaged vegetation
61 decreases isoprene emissions and stomatal conductance (Wittig et al., 2009; Feng et
62 al., 2019), which influence O₃ production and dry deposition. Moreover, weakened
63 leaf-level transpiration following O₃ damage modulates meteorological parameters,
64 such as surface air temperature and atmospheric relative humidity, leading to
65 substantial biogeophysical feedbacks on surface O₃ (Lombardozzi et al., 2012; Sadiq
66 et al., 2017).

67
68 Interactions between air pollution and terrestrial ecosystems remain challenging due
69 to limited process-based knowledge and the separate development of chemistry and
70 vegetation models (He et al., 2020). At present, the feedbacks from O₃-damaging

Moved down [1]: Fire plays an important role in disturbing the terrestrial carbon budget (Bond-Lamberty et al., 2007; Amiro et al., 2009; Turetsky et al., 2011; Yue and Unger, 2018). Global fires directly emit 2-3 Pg (1 Pg = 10¹⁵ g) carbon into the atmosphere every year (van der Werf et al., 2010). M

Deleted: Moreover, fires contribute to the production of tropospheric ozone (O₃)...

Moved down [2]: by emitting substantial number of precursors (Cheng et al., 1998; Kita et al., 2000; Oltmans et al., 2010; Jaffe et al., 2013; Lu et al., 2016). Globally, fires account for 3-5% of the total tropospheric O₃ (Bey et al., 2001; Ziemke et al., 2009; Jaffe and Wigder, 2012). R

Deleted: Regionally, the influence of fires on O₃ production is dependent on mixing with urban emissions Tropospheric

Deleted: Jaffe

Deleted: 2004; Singh et al., 2010

Deleted: . In some areas, fires can enhance surface O₃ by 10-30 ppbv through emissions of NO_x and VOCs (McKeen et al., 2002; Pfister et al., 2008; Yue and Unger, 2018). Model simulations project that future wildfire activity will likely increase due to global warming, suggesting an increased risk of surface O₃ from wildfires (Amiro et al., 2009; Balshi et al., 2009; Wang et al., 2016; Yue et al., 2017).¶

¶
Tropospheric O₃ is a toxic air pollutant with detrimental effects on vegetation (Yue and Unger, 2014)...

Deleted: Modeling studies estimated that fire-induced O₃ reduces global GPP by 0.7% with regional maximum reductions of >4.0% over central Africa (Yue and Unger, 2018). In turn, vegetation ...

Deleted: Emissions from biomass burning generate a large amount of O₃ precursors (Jaffe and Wigder, 2012; Lu et al., 2016). Moreover, vegetation acts as an important sink for tropospheric O₃ through stomatal uptake ...

Deleted: Wesely and Hicks, 2000; Val Martin

Deleted: 2014

Deleted: . Globally, stomatal uptake contributes to 40-60% of the canopy total O₃ deposition (Fowler et al., 2009)...

110 vegetation on O₃ have only been examined by four papers (Sadiq et al., 2017; Zhou et
111 al., 2018; Gong et al., 2020; Zhu et al., 2021), Sadiq et al. (2017), implemented a
112 parameterization of O₃ vegetation damage into a climate model and quantified online
113 O₃-vegetation coupling. Simulations showed that surface O₃ could be enhanced by up
114 to 4-6 ppbv over Europe, North America, and China through comparable effects from
115 biogeochemical (decreased dry deposition and increased isoprene emissions) and
116 biogeophysical (changes in meteorological variables following reduced transpiration
117 rate) feedbacks from O₃-vegetation interactions. Similar conclusions were achieved
118 by Zhu et al. (2021), who investigated the effects of O₃-vegetation interaction in
119 China using a two-way coupled land-atmosphere model. By including O₃ damage to
120 isoprene emissions in a fully coupled global chemistry-carbon-climate model, Gong
121 et al. (2020) highlighted that such O₃-vegetation positive feedbacks were mainly
122 driven by reduced dry deposition following O₃ damage to photosynthesis. Different
123 from above three studies, Zhou et al. (2018) implemented steady-state O₃-induced
124 LAI changes into GEOS-Chem and quantified only the influences of O₃-vegetation
125 biogeochemical feedbacks because the model is driven with prescribed
126 meteorological fields. Results showed that O₃-induced damage to LAI can enhance O₃
127 by up to 3 ppbv in the tropics, eastern North America, and southern China through
128 changes in dry deposition and isoprene emissions. All studies revealed strong positive
129 O₃-vegetation feedback to surface O₃, though the magnitudes are different due to
130 discrepancies in O₃ damaging schemes, as well as differences in the models.

Deleted: three papers. By implementing steady-state O₃-induced LAI changes into a chemical transport model, ...

Deleted: . (

Deleted: quantified the influences of O₃-vegetation feedback and found that O₃-induced damage to LAI can enhance O₃ by up to 3 ppbv in the tropics, eastern North America, and southern China. Moreover, plant stomatal conductance may decrease to prevent excessive O₃ from entering plants ...

Deleted: (Manninen

Deleted: ., 2003; Wittig et al., 2009

Deleted: . Consequently, surface O₃ may increase due to reduced dry deposition (Val Martin et al., 2014; Lin et al., 2019). Sadiq et al. (2017) implemented a parameterization of O₃ vegetation damage into a climate model and quantified online O₃-vegetation coupling. Simulation results showed that surface O₃ can be enhanced by up to 4-6 ppbv over Europe, North America, and China mainly because of reduced dry deposition velocity following O₃ damage. Similarly, Gong et al. (2020) used a fully coupled chemistry-carbon-climate global model and found that O₃-induced inhibition of stomatal conductance can increase surface O₃ by 1.4-2.1 ppbv in eastern China and 1.0-1.3 ppbv in western Europe. All studies revealed strong positive O₃-vegetation feedback to surface O₃, although the magnitudes are different due to discrepancies in O₃ damaging schemes, as well as differences in the climate...

131

158 Fire plays an important role in disturbing the terrestrial carbon budget
159 (Bond-Lamberty et al., 2007; Amiro et al., 2009; Turetsky et al., 2011; Yue and Unger,
160 2018). Global fires directly emit 2-3 Pg (1 Pg = 10¹⁵ g) carbon into the atmosphere
161 every year (van der Werf et al., 2010). Moreover, fires contribute to the production of
162 tropospheric O₃ by emitting substantial number of precursors (Cheng et al., 1998; Kita
163 et al., 2000; Oltmans et al., 2010; Jaffe et al., 2013; Lu et al., 2016). Globally, fires
164 account for 3-5% of the total tropospheric O₃ (Bey et al., 2001; Ziemke et al., 2009;
165 Jaffe and Wigder, 2012). Regionally, especially in Amazon and central Africa, fires
166 can enhance surface O₃ by 10-30 ppbv through emissions of NO_x and VOCs during
167 fire seasons (Yue and Unger, 2018; Pope et al., 2020). Over these regions, strong
168 O₃-vegetation interactions are expected because of high fire O₃ concentrations and
169 dense vegetation cover. Previous studies showed that fire O₃ causes large GPP
170 reduction of 200-400 Tg C yr⁻¹ over Amazon and central Africa (Pacifico et al., 2015;
171 Yue and Unger, 2018). With likely increased wildfire activity due to global warming,
172 surface O₃ will be further enhanced by wildfires (Amiro et al., 2009; Balshi et al.,
173 2009; Wang et al., 2016; Yue et al., 2017), leading to more severe O₃ damage on
174 vegetation. Although the feedback of vegetation damage on surface O₃ have been well
175 explored on global (Sadiq et al., 2017; Zhou et al., 2018; Gong et al., 2020) or
176 regional (Zhu et al., 2021) scales, these studies all focused on O₃-vegetation from
177 combined anthropogenic and natural sources. Therefore, quantification of the
178 O₃-vegetation interactions associated with fire emissions is very important for a
179 comprehensive understanding of the effects of fires on surface O₃.

Moved (insertion) [1]

Moved (insertion) [2]

Deleted: Many studies have quantified the direct contributions of fires to tropospheric O₃ ...

Formatted: Font color: Auto

Deleted: (Martin et al., 2006; Pfister et al., 2006; Ziemke et al., 2009; Yokelson et al., 2011; Jaffe and Wigder, 2012; Larsen et al., 2018; Yue and Unger, 2018)(Yue and Unger,

Deleted: . However, the feedback of fire-induced O₃ vegetation damage to surface O₃ remain unquantified. ...

187

188 Here, we apply a fully coupled chemistry-vegetation model (GEOS-Chem-YIBs,
189 hereafter referred to as GC-YIBs) to examine the indirect contributions of fires to
190 surface O₃. Fire-induced O₃ affects plant photosynthesis and stomatal conductance. In
191 turn, predicted changes in LAI and canopy stomatal conductance influence both the
192 sources and sinks of tropospheric O₃. Such O₃-vegetation interactions result in
193 additional enhancement in surface O₃ caused by fire emissions (Fig. 1). Section 2
194 describes the GC-YIBs model and sensitivity experiments conducted in this study.
195 Section 3 quantifies the feedbacks of fire-induced O₃ vegetation damage on surface
196 O₃ concentrations. The last section summarizes the findings and discusses the
197 uncertainties.

198

199 **2 Materials and Methods**

200 **2.1 The GC-YIBs model**

201 GC-YIBs is a coupled chemistry-vegetation model developed by implementing the
202 Yale Interactive terrestrial Biosphere (YIBs) model into GEOS-Chem version 12.0.0
203 (Lei et al., 2020). GEOS-Chem is a widely used global 3-D chemical transport model
204 (CTM) for simulating atmospheric composition and air quality (Yue et al., 2015; Yan
205 et al., 2018; David et al., 2019; Lu et al., 2019). This model uses a detailed
206 HO_x-NO_x-VOC-O₃-halogen-aerosol tropospheric chemistry to simulate tropospheric
207 O₃ fluxes (Barret et al., 2016; Gong and Liao, 2019), while a simplified linearized
208 Linoz chemistry mechanism is applied to simulate stratospheric O₃ (McLinden et al.,

209 2000). Aerosols simulated in GEOS-Chem include secondary inorganic aerosols,
210 secondary organic aerosols, primary organic aerosols, black carbon, dust, and sea salt
211 (Dang and Liao, 2019; Li et al., 2019). The gas-aerosol partitioning of the sulfate–
212 nitrate–ammonium system is computed by the ISORROPIA v2.0 thermodynamic
213 equilibrium model (Fountoukis and Nenes, 2007). The atmospheric emissions from
214 different sources, regions, and species on a user-defined grid are calculated through
215 the online Harvard NASA Emissions Component (HEMCO) module (Keller et al.,
216 2014). HEMCO is highly customizable in that it can automatically combine, overlay,
217 and update emission inventories and scale factors specified by the users. In general,
218 the GEOS-Chem model overestimates summer surface O₃ concentrations in the
219 eastern U.S. and China (Zhang et al., 2011; Travis et al., 2016; Schiferl and Heald,
220 2018).

221

222 YIBs is a vegetation model designed to dynamically simulate the changes in LAI and
223 tree height based on carbon assimilation, respiration, and allocation processes (Yue
224 and Unger, 2015). The model computes carbon uptake for 9 vegetation types,
225 including evergreen needleleaf forest, deciduous broadleaf forest, evergreen broadleaf
226 forest, shrubland, tundra, C₃/C₄ grasses, and C₃/C₄ crops. The canopy is divided into
227 an adaptive number of layers (typically 2-16) for light stratification. The YIBs model
228 applies a well-established Michaelis–Menten enzyme kinetics scheme to compute the
229 leaf photosynthesis (Farquhar et al., 1980; Von Caemmerer and Farquhar, 1981).
230 which is further upscaled to the canopy level by the separation of sunlit and shaded

Deleted: for C₃ and C₄ plants

Deleted: . The leaf stomatal conductance was calculated based on the model of Ball and Berry (Baldocchi et al., 1987). The Spitters (1986) canopy radiative transfer scheme is used to separate light use processes for sunlit and shaded leaves.,

236 [leaves \(Spitters, 1986\)](#). The LAI and carbon allocation schemes are from the TRIFFID
237 model (Clark et al., 2011). Previous studies have shown that the YIBs model has good
238 performance in simulating the spatial pattern and temporal variability of GPP and LAI
239 based on site observations and satellite products (Yue and Unger, 2015, 2018).

Formatted: Font color: Text 1

240

241 The GC-YIBs model links atmospheric chemistry and vegetation in a two-way
242 coupling. As a result, changes in chemical components or vegetation will
243 simultaneously feed back to influence the other systems. In this study, the GC-YIBs
244 model is driven with the meteorological fields from the Modern-Era Retrospective
245 analysis for Research and Applications, version 2 (MERRA2) with a horizontal
246 resolution of 4° latitude by 5° longitude, as well as 47 vertical layers from the surface
247 to 0.01 hPa. Within GC-YIBs, the online-simulated surface O₃ in GEOS-Chem affects
248 photosynthesis and canopy stomatal conductance; in turn, the online-simulated
249 vegetation parameters, such as LAI and stomatal conductance, in YIBs, affect both the
250 sources and sinks of O₃ by altering precursor emissions and dry deposition at the
251 1-hour integration time step. An earlier study evaluated the GC-YIBs model and
252 showed good performance in simulating surface O₃, GPP, LAI, and O₃ dry deposition
253 (Lei et al., 2020).

254

255 **2.2 Scheme of O₃ vegetation damage**

256 The GC-YIBs model calculates the impacts of O₃ exposure on photosynthesis based
257 on a semi-mechanistic scheme (Sitch et al., 2007):

$$A' = \alpha \cdot A \quad (1)$$

where A' and A represent the O_3 -damaging and original leaf photosynthesis, respectively. The O_3 damage factor is represented by α ; O_3 can cause damage to photosynthesis only if $\alpha < 1$. The factor α is calculated as a function of excessive O_3 flux and damaging sensitivity coefficient (β):

$$\alpha = -\beta \cdot \max(F_{O_3} - T_{O_3}, 0) \quad (2)$$

The coefficient β can have two values for each vegetation type (Table S1), indicating low to high O_3 damaging sensitivities (Sitch et al., 2007). T_{O_3} represents the O_3 flux threshold, reflecting the O_3 tolerance of different vegetation types. F_{O_3} represents the stomatal O_3 flux and is calculated based on ambient $[O_3]$, aerodynamic resistance (r_a), boundary layer resistance (r_b) and stomatal resistance (r_s):

$$F_{O_3} = \frac{[O_3]}{r_a + r_b + k \cdot r_s'} \quad (3)$$

Here k represents the ratio of leaf resistance for O_3 to leaf resistance for water vapor. Parameters r_a and r_b are calculated by the GEOS-Chem model. O_3 -damaging leaf photosynthesis (A') is then integrated over all canopy layers to generate O_3 -damaging GPP:

$$GPP' = \int_0^{LAI} A' dL \quad (4)$$

The O_3 -damaging stomatal resistance (r_s') is calculated based on the model of Ball and Berry (Baldocchi et al., 1987):

$$\frac{1}{r_s'} = g_s' = m \frac{A'_{net} RH}{c_s} + b \quad (5)$$

where m and b represent the slope and intercept of empirical fitting to the Ball-Berry stomatal conductance equation, respectively. A'_{net} represents

Formatted: Indent: First line: 13 ch

Deleted: 4

281 O₃-damaging net leaf photosynthesis, *RH* represents the relative humidity and c_s is
282 the ambient CO₂ concentration. Previous studies have shown that this scheme within
283 the framework of YIBs can reasonably capture the response of GPP and stomatal
284 conductance to surface [O₃] based on hundreds of global observations (Yue et al.,
285 2016; Yue and Unger, 2018).

286

287 **2.3 Fire emissions**

288 Fire Inventory from NCAR (FINN) version 1.5 is used by GC-YIBs to simulate
289 fire-induced perturbations in O₃. FINN provides daily global emissions of many
290 chemical species from open biomass burning at a resolution of 1 km² (Wiedinmyer et
291 al., 2011). The inventory estimates fire locations and biomass burned using satellite
292 observations of active fires and land cover, together with emission factors and fuel
293 loadings. For each land type, emission factors for different gaseous and particulate
294 species are taken from measurements (Andreae and Merlet, 2001; Andreae and
295 Rosenfeld, 2008; Akagi et al., 2011). Daily fire emissions for 2002-2012 are available
296 at <http://bai.acom.ucar.edu/Data/fire/>. In GC-YIBs, all biomass burning emissions
297 occur in the atmospheric boundary layer. Such configuration might slightly
298 overestimate regional O₃ formation as observations suggested ~20% of fire plumes
299 reached the height above the boundary layer (Val Martin et al., 2010) and
300 consequently enhanced surface O₃ level at the downwind regions (Jaffe and Wigder,
301 2012). The FINN inventory has been widely used in regional and global chemical
302 transport models (e.g., WRF-Chem and GEOS-Chem) to quantify the impacts of fires

Deleted: Daily fire emissions for 2002-2012 are available at <http://bai.acom.ucar.edu/Data/fire/>. In GC-YIBs, all biomass burning emissions are emitted into the atmospheric boundary layer. Daily fire emissions for 2002-2012 are avai

307 on air quality and weather (Jiang et al., 2012; Nuryanto, 2015; Vongruang et al., 2017;
308 Brey et al., 2018; Watson et al., 2019).

309

310 **2.4 Site-level measurements**

311 Measurements of surface [O₃] in the U.S. are provided by Air Quality System (AQS,
312 <https://www.epa.gov/aqs>), those over Europe are provided by European Monitoring
313 and Evaluation Programme (EMEP, <https://emep.int>). The observed [O₃] at Manaus,
314 Tg Malim, and Welgegund sites are from earlier studies (Ahamad et al., 2014; Laban
315 et al., 2018; Pope et al., 2020).

316

317 **2.5 Model simulations**

318 In this study, eight simulations (Table 1) are performed to examine both the direct and
319 indirect contributions of fires to surface O₃. These simulations can be divided into two
320 main groups:

- 321 1. CTRL_FIRE and CTRL_NOFIRE are the control runs using the same emissions
322 except that the latter omits fire emissions. These runs calculate and output offline
323 O₃ damage, which decreases instantaneous leaf photosynthesis but does not feed
324 back to affect plant growth and O₃ dry deposition.
- 325 2. O3CPL_FIRE and O3CPL_NOFIRE are the sensitive experiments that consider
326 online coupling between O₃ and vegetation. These runs include online O₃ damage
327 to plant photosynthesis, which feeds back to affect both vegetation and air
328 pollution. The two simulations apply the same emissions, except that the latter

329 omits fire emissions.

330

331 For each of these four configurations, two runs are conducted with either high (HS) or
332 low (LS) O₃ damaging sensitivities. All simulations are performed from 2002-2012
333 using the GC-YIBs model driven by MERRA2 meteorological fields. The first 3 years
334 are used as spin up, and the results of the last 8 years are analyzed. For the same
335 configurations, the results from low and high O₃ damaging sensitivities are averaged.
336 The differences between CTRL_NOFIRE and O3CPL_NOFIRE represent the surface
337 O₃ enhancements through O₃-vegetation feedback without fire emissions. The
338 differences between CTRL_FIRE and CTRL_NOFIRE, named O3OFF, represent the
339 direct contributions of fires to surface O₃. The differences between O3CPL_FIRE and
340 O3CPL_NOFIRE, named O3CPL, represent both direct and indirect contributions of
341 fires to surface O₃. The differences between O3CPL and O3OFF represent the indirect
342 contributions of fires to surface O₃ through O₃-vegetation interactions. It should be
343 noted that only biogeochemical feedbacks from O₃ vegetation damage on surface O₃
344 are considered in this study because GC-YIBs uses prescribed meteorology
345 (MERRA2).

346

347 **3 Results**

348 **3.1 Model validation**

349 Simulated surface daily maximum 8-hour average O₃ concentrations (MDA8 [O₃],
350 short for [O₃] hereafter) are evaluated using measurements from the AQS and EMEP

351 datasets over the period of 2005-2012 (Fig 2). The model well captures the observed
352 spatial distribution of annual $[O_3]$ in the U.S. and Europe, with a high correlation
353 coefficient of 0.51 ($p < 0.01$). Although GC-YIBs overestimates the $[O_3]$ in the eastern
354 U.S. while underestimating it in western Europe, the normalized mean bias (NMB) is
355 only 4.0%, with a root mean square error (RMSE) of 5.4 ppbv. Therefore, the
356 simulated O_3 vegetation damage in our study is slightly overestimated in the eastern
357 U.S. but underestimated in western Europe.

358

359 3.2 Direct contributions of fires to O_3

360 Without fire emissions, the simulated global mean $[O_3]$ is 23.9 ppbv, with a grid
361 maximum of 63.7 ppbv over the Beijing–Tianjin–Hebei region averaged for
362 2005-2012 (Fig. 3a). Most high $[O_3]$ is distributed in the Northern Hemisphere, where
363 anthropogenic emissions make the dominant contributions. The inclusion of fire
364 emissions increases global annual $[O_3]$ by an average of 1.2 ppbv (5.0%). Regionally,
365 the largest enhancement of $[O_3]$ by 5.9 ppbv (24.4%) is averaged over central Africa,
366 with smaller enhancements of 5.7 ppbv (38.2%) averaged over the Amazon, and 3.8
367 ppbv (10.2%) averaged over southern Asia. Smaller enhancements of 1.1 ppbv (2.2%),
368 0.9 ppbv (2.1%), and 0.8 ppbv (2.2%) are averaged respectively over eastern China,
369 western Europe, and the eastern U.S. (Fig. 3b). The predicted fire-induced
370 enhancements in $[O_3]$ agree well with the simulations using the same model but with
371 fire emissions from the Global Fire Emission Database (GFED) version 3 (Yue and
372 Unger, 2018).

Deleted: annual

374

375 We further evaluated the model performance in simulating fire-induced $\Delta[\text{O}_3]$ at three
376 sites across biomass burning regions (Fig. S1). Without fire emissions, the $[\text{O}_3]$ is
377 obviously underestimated, with NMBs of -25.5% at Tg Malim, -53.6% at Manaus,
378 and -21.3% at Welgegund. As a comparison, simulations with fire emissions show
379 NMBs in fire seasons of -8.7% at Tg Malim, -1.4% at Manaus, and -15.1% at
380 Welgegund, suggesting improved O_3 simulations by including fire emissions.

381

382 3.3 Fire-induced O_3 damages to GPP

383 Surface O_3 causes strong damage to ecosystem productivity (Fig. 4). Without fire
384 emissions, surface O_3 reduces global annual GPP by 1.7% (3899.8 Tg C yr⁻¹, Figs. 4a
385 and 4c). Regional maximum reductions of 10.9% (372.0 Tg C yr⁻¹), 6.1% (366.1 Tg C
386 yr⁻¹), and 4.9% (323.8 Tg C yr⁻¹) are averaged respectively over eastern China, the
387 eastern U.S., and western Europe; these reductions are attributed to the high ambient
388 $[\text{O}_3]$ level and the large stomatal conductance over these regions. The patterns of
389 O_3 -induced GPP reductions agree with previous estimates using the same O_3 damage
390 schemes (Sitch et al., 2007; Yue and Unger, 2015). However, compared to simulations
391 using another scheme (Lombardozzi et al., 2012; Zhou et al., 2018; Zhu et al., 2021),
392 this study estimates smaller GPP reductions. Such discrepancy indicates there are
393 large uncertainties in O_3 vegetation damage schemes, and more observations should
394 be developed to evaluate different schemes in future studies.

395

Deleted: different models

397 The inclusion of fire emissions causes additional GPP reductions. Globally,
398 fire-induced ΔO_3 decreases annual GPP by 0.4% (1312.0 Tg C yr⁻¹, Figs. 4b and 4d).
399 Regionally, the largest GPP reduction of 1.4% (370.3 Tg C yr⁻¹) is averaged over the
400 Amazon due to the largest enhancement of [O₃] caused by fires. Furthermore, fire
401 $\Delta[O_3]$ causes additional annual GPP reductions of 1.3% (358.0 Tg C yr⁻¹), averaged
402 over central Africa, and 1.0% (77.1 Tg C yr⁻¹), averaged over southern Asia. In
403 contrast, limited damage is found in eastern China, western Europe, and the eastern
404 U.S. due to low fire $\Delta[O_3]$. Following the changes in GPP, fire-induced O₃ damage to
405 LAI shows a regional maximum of 0.3-0.7% in central Africa and a global reduction
406 of 0.02-0.5% (Fig. S2).

Formatted: Font: Not Bold

407

408 **3.4 Indirect contributions of fires to O₃**

409 Vegetation parameters such as LAI and stomatal conductance play important roles in
410 modulating surface [O₃]. The O₃-induced changes in these variables interactively feed
411 back to alter local [O₃] (Fig. 5). Without fire emissions, the annual $\Delta[O_3]$ from
412 O₃-vegetation interactions is limited to eastern China by 0.5 ppbv, the eastern U.S. by
413 0.3 ppbv, and western Europe by 0.2 ppbv. The largest grid positive feedback of up to
414 0.8 ppbv is found in the eastern U.S. (Figs. 5a and 5c). Sensitivity experiments further
415 show that such enhancement of surface [O₃] mainly results from the inhibition of
416 stomatal conductance following reduced photosynthesis by O₃ damage (Fig. S3a).

Deleted: stomatal uptake

417 Consequently, large $\Delta[O_3]$ (Figs. 5a and 5c) are collocated with areas enduring high
418 levels of O₃ vegetation damage (Figs. 4a and 4c). As a comparison, the feedback of

Deleted:), which reduces the O₃ dry deposition velocity (Fig. S4...

422 LAI changes is generally small (Fig. S3b), which is mainly attributed to limited O₃
423 damage on LAI (Fig. S2). The enhancement of [O₃] from fires causes additional
424 feedback to the surface [O₃]. The largest annual Δ [O₃] of 0.13 ppbv due to
425 O₃-vegetation feedback is averaged on over the Amazon (Figs. 5b and 5d), where the
426 highest GPP reductions by fire-induced O₃ are predicted (Figs. 4b and 4d). Such
427 feedback additionally enhances local [O₃] by 0.12 ppbv, averaged over central Africa,
428 and 0.09 ppbv, averaged over southern Asia. However, limited O₃-vegetation feedback
429 is found in the eastern U.S., eastern China, and western Europe, either because of low
430 fire-induced Δ [O₃] (Fig. 3b) or low Δ GPP (Figs. 4b and 4d). The changes in O₃ dry
431 deposition velocity broadly match the pattern of O₃-vegetation feedback (Fig. S4),
432 suggesting that reduced dry deposition velocity due to O₃-induced inhibition of
433 stomatal conductance is the dominant driver for the enhanced surface [O₃].

434

435 Fig. 6 shows seasonal variations in O₃-vegetation feedback. Without fire emissions,
436 O₃-vegetation feedback in eastern China, the eastern U.S., and western Europe shows
437 similar seasonal variations, increasing from January to July and then decreasing (Fig.
438 6a). For these regions, surface [O₃] and stomatal conductance reach maximums during
439 the growth season (May-October), resulting in instantaneous O₃ uptake. Therefore,
440 O₃-vegetation interactions are expected to be stronger during the growth season in the
441 Northern Hemisphere. However, O₃-vegetation feedback driven by fires in the
442 Amazon and Southern Asia reaches a maximum during August-December and
443 February-June, respectively. Moreover, double peaks are shown in central Africa, with

444 maximums during February-April and July-September (Fig. 6b). The distinct seasonal
445 variations in biomass burning regions are attributed to fire emissions. At low latitudes,
446 stomatal conductance shows limited seasonal variations. Therefore, O₃-vegetation
447 feedback driven by fires is mainly dependent on fire-induced $\Delta[\text{O}_3]$.

448

449 Fire-induced O₃ shows stronger interactions with vegetation under favorable
450 meteorological conditions. We sort daily $\Delta[\text{O}_3]$ from O₃-vegetation feedback and
451 calculate the average of $\Delta[\text{O}_3]$ above the 95th percentile (Fig. S5). The spatial pattern
452 of $\Delta[\text{O}_3]$ during extreme O₃-vegetation feedback is broadly consistent with that of the
453 annual average, albeit with much stronger O₃-vegetation feedback. Without fire
454 emissions, O₃-vegetation feedback enhances [O₃] by 2.0 ppbv averaged over eastern
455 China, 1.8 ppbv averaged over the eastern U.S., and 1.1 ppbv averaged over western
456 Europe (Figs. S5a and S5c). Fire emissions alone enhance [O₃] through O₃-vegetation
457 interactions by 1.1 ppbv averaged over the Amazon, 0.8 ppbv averaged over southern
458 Asia, and 0.6 ppbv averaged over central Africa during extreme O₃-vegetation
459 feedback (Figs. S5b and S5d).

460

461 **3.5 Indirect vs. direct contributions of fires to O₃**

462 We further compare the indirect and direct contributions of fire emissions to surface
463 [O₃]. Here, the direct contributions indicate $\Delta[\text{O}_3]$ caused by fire emissions of
464 chemical precursors, while the indirect contributions represent additional $\Delta[\text{O}_3]$ from
465 O₃-vegetation interactions caused by fire-induced O₃. Without fire emissions,

466 O₃-vegetation interactions cause enhancement of [O₃] by 1.0% averaged over eastern
467 China, 0.8% averaged over the eastern U.S., and 0.5% averaged over western Europe
468 (Figs. 7a and 7c). Compared to nonfire sources, fire emissions cause larger relative
469 perturbations in surface [O₃] through O₃-vegetation interactions (Figs. 7b and 7d).
470 The ratios of indirect to direct annual Δ[O₃] are 3.7% averaged over eastern China,
471 2.0% averaged over the eastern U.S., and 1.6% averaged over western Europe. For
472 these regions, the absolute Δ[O₃] from direct fire emissions is usually lower than 1
473 ppbv (Fig. 3b). However, the high level of background [O₃] (all sources except fire
474 emissions, Fig. 3a) provides such a sensitive environment that the moderate increases
475 of [O₃] from fires can cause large feedback to regional surface [O₃] through
476 vegetation damage. For fire-prone regions, the ratios of indirect to direct annual Δ[O₃]
477 are 2.6% averaged over southern Asia, 1.9% averaged over the eastern U.S., and 1.4%
478 averaged over central Africa.

479

480 3.6 Aggravated O₃ damage to GPP through O₃-vegetation feedback

481 The additional O₃ enhancement can exacerbate the damaging effects on vegetation.
482 Without fire emissions, online O₃ causes a global annual GPP reduction of 0.2%
483 (299.6 Tg C yr⁻¹, Figs. S6a and S6c) from the offline O₃. Regionally, additional
484 reductions are mainly found in eastern China, the eastern U.S., and western Europe,
485 where GPP is further decreased by 27.1 Tg C yr⁻¹, 40.8 Tg C yr⁻¹ and 28.4 Tg C yr⁻¹,
486 respectively. For fire emissions, the online fire-induced ΔO₃ results in a higher GPP
487 reduction by 25.0 Tg C yr⁻¹ averaged over the Amazon, and 24.3 Tg C yr⁻¹ averaged

Deleted: ambient

Deleted: in which

Deleted: in

Deleted: indirect contributions

492 over central Africa, and 7.1 Tg C yr⁻¹ averaged over southern Asia compared to the
493 offline fire-induced ΔO_3 (Figs. S6b and S6d). Such spatial patterns are broadly
494 consistent with $\Delta[\text{O}_3]$ induced by O_3 -vegetation feedback (Fig. 5).

495

496 **4 Conclusions and discussion**

497 Many studies have explored the direct contributions to surface O_3 by fire emissions.
498 However, the feedback of fire-induced O_3 vegetation damage to surface $[\text{O}_3]$ remains
499 unquantified. In this study, we find that fire-induced O_3 causes a positive feedback to
500 surface $[\text{O}_3]$ mainly because of the inhibition effects on stomatal conductance.

501 Regionally, O_3 -vegetation feedback driven by fires enhances surface annual $[\text{O}_3]$ by
502 0.13 ppbv averaged over the Amazon, 0.12 ppbv averaged over central Africa, and
503 0.09 ppbv averaged over southern Asia. Such feedback exhibit large seasonal
504 variations, with the maximums of 0.5 ppbv averaged over the Amazon in October, 0.3
505 ppbv averaged over southern Asia in April, and 0.2 ppbv averaged over central Africa
506 in April. During extreme O_3 -vegetation interactions, the feedback can rise to >0.6
507 ppbv in these fire-prone areas. Although direct formations of O_3 from fires are limited
508 in eastern China and the eastern U.S., the feedback of O_3 -vegetation coupling results
509 in additional enhancement of surface $[\text{O}_3]$ by 3.7% and 2.0% upon the fire-induced
510 $\Delta[\text{O}_3]$. Such large ratios in these regions are attributed to the high level of ambient $[\text{O}_3]$
511 that provides a sensitive environment in which moderate increases in $[\text{O}_3]$ from fires
512 can cause large indirect contributions to regional $[\text{O}_3]$ through vegetation damage.

513

514 Some uncertainties may affect the conclusions of this study. (i) The GC-YIBs
515 simulations do not consider the direct fire damages to vegetation and the consequent
516 long-term recovery of forests. In our study, we focus only on the feedbacks of
517 fire-induced O₃-vegetation interactions to surface O₃. (ii) Fires can decrease VOC
518 emissions from biogenic sources by damaging vegetation directly. However,
519 compared to the VOCs emitted by fires, the VOC loss from burned vegetation is
520 generally smaller (Fig. S7). Therefore, the influence of reduced VOCs from
521 vegetation loss on surface [O₃] can be ignored. (iii) There is evidence that O₃
522 exposure may cause “sluggishness” that delays the stomatal responses to O₃ damage
523 (Huntingford et al., 2018). However, we do not include “sluggishness” in our scheme
524 because its net impacts on stomatal conductance remain uncertain. For example,
525 observations found that the increased short-term water loss (delayed stomatal
526 responses) may be offset by the decreased long-term water loss (lower steady-state
527 stomatal conductance) with the stomatal “sluggishness” (Paoletti et al., 2019). (iv) We
528 employed a model resolution of 4°×5° due to the limitations in computational
529 resources. We performed a one-year sensitivity simulation at a 2°×2.5° resolution.
530 The comparisons show that fire-induced direct O₃ enhancement is very similar
531 between the simulations with low and high resolutions, although the former runs
532 predict slightly higher changes in [O₃] than the latter (Fig. S8). (v) different biomass
533 burning datasets may affect the estimated O₃-vegetation feedback in our study. At
534 present, the FINNv1.5 and GFEDv4.1 inventories are available in the public-release
535 of GEOS-Chem v12.0.0. Compared with the FINNv1.5 inventory, simulations using

Moved (insertion) [3]

Deleted: First, we

Deleted: S7). Second,

538 the GFEDv4.1 inventory predict a lower O₃-vegetation feedback in the Amazon (Fig.
539 [S9a](#)) and southern Asia (Fig. [S9c](#)) but a higher O₃-vegetation feedback in central
540 Africa (Fig. [S9b](#)).

541
542 Despite these uncertainties, we present the first estimate of O₃ enhancement by fire
543 emissions through O₃-vegetation interactions. Such enhancement is not limited to
544 fire-prone regions, but is also significant over downwind areas with high ambient [O₃]
545 levels. Although the absolute perturbations may be moderate for the whole fire season,
546 O₃-vegetation interactions can largely increase surface O₃ during extreme
547 O₃-vegetation interactions, leading to additional threats to public health and
548 ecosystem productivity.

549

550 **Data availability**

551 The site-level [O₃] in the U.S. can be download from AQS (<https://www.epa.gov/aqs>).
552 The site-level [O₃] in the Europe can be download from EMEP (<https://emep.int>). The
553 observed [O₃] at Manaus, Tg Malim, and Welgegund sites are from earlier studies
554 (Ahamad et al., 2014; Laban et al., 2018; Pope et al., 2020). The GC-YIBs simulation
555 results are available from the corresponding authors on request.

556

557 **Competing interests.** The authors declare no competing financial interests.

558

Deleted: S8a

Deleted: S8c

Moved up [3]: . However, compared to the VOCs emitted by fires, the VOC loss from burned vegetation is generally smaller (Fig. S

Deleted: S8b). Finally, fires can decrease VOC emissions from biogenic sources by burning vegetation...

Deleted: S9). Therefore, the influence of reduced VOCs from vegetation loss on surface [O₃] can be ignored....

568 **Author Contributions.** XY conceived the study. YL conducted the model
569 simulations. YL and XY were responsible for results analysis. HL, LZ, and YY
570 revised and improved the manuscript. HZ, CT, and CG helped prepare model input.
571 YM, LG, and YC helped prepare observation dataset.

572

573 **Acknowledgements.** This work was jointly supported by Jiangsu Science Fund for
574 Distinguished Young Scholars (grant no. BK20200040) and the National Natural
575 Science Foundation of China (grant no. 41975155).

576

577

578 **References**

579 Ahamad, F., Latif, M. T., Tang, R., et al. Variation of surface ozone exceedance around Klang Valley,
580 Malaysia. Atmospheric research[J]: 2014, 139: 116-127.
581 Ainsworth, E. A., Yendrek, C. R., Sitch, S., et al. The Effects of Tropospheric Ozone on Net Primary
582 Productivity and Implications for Climate Change. Annual Review of Plant Biology, Vol 63[J]: 2012, 63:
583 637-661.
584 Akagi, S., Yokelson, R. J., Wiedinmyer, C., et al. Emission factors for open and domestic biomass
585 burning for use in atmospheric models. Atmospheric Chemistry and Physics[J]: 2011, 11: 4039-4072.
586 Akhtar, N., Yamaguchi, M., Inada, H., et al. Effects of ozone on growth, yield and leaf gas exchange
587 rates of two Bangladeshi cultivars of wheat (Triticum aestivum L.). Environmental Pollution[J]: 2010,
588 158: 1763-1767.
589 Amiro, B. D., Cantin, A., Flannigan, M. D., et al. Future emissions from Canadian boreal forest fires.
590 Canadian Journal of Forest Research[J]: 2009, 39: 383-395.
591 Andreae, M. and Rosenfeld, D. Aerosol–cloud–precipitation interactions. Part 1. The nature and
592 sources of cloud-active aerosols. Earth-Science Reviews[J]: 2008, 89: 13-41.
593 Andreae, M. O. and Merlet, P. Emission of trace gases and aerosols from biomass burning. Global
594 biogeochemical cycles[J]: 2001, 15: 955-966.
595 Baldocchi, D. D., Hicks, B. B. and Camara, P. A Canopy Stomatal-Resistance Model for Gaseous
596 Deposition to Vegetated Surfaces. Atmospheric Environment[J]: 1987, 21: 91-101.
597 Barret, B., Sauvage, B., Bennouna, Y., et al. Upper-tropospheric CO and O₃ budget during the Asian
598 summer monsoon. Atmos. Chem. Phys[J]: 2016, 16: 9129-9147.
599 Bey, I., Jacob, D. J., Logan, J. A., et al. Asian chemical outflow to the Pacific in spring: Origins, pathways,
600 and budgets. Journal of Geophysical Research-Atmospheres[J]: 2001, 106: 23097-23113.

Deleted:),

Deleted:), and the National Key Research and Development Program of China (grant nos. 2019YFA0606802 and 2017YFA0603802)

Formatted: Font: 10.5 pt

605 Bond-Lamberty, B., Peckham, S. D., Ahl, D. E., et al. Fire as the dominant driver of central Canadian
606 boreal forest carbon balance. *Nature*[J]: 2007, 450: 89-92.

607 Booker, F. L., Burkey, K. O., Pursley, W. A., et al. Elevated carbon dioxide and ozone effects on peanut: I.
608 Gas-exchange, biomass, and leaf chemistry. *Crop Science*[J]: 2007, 47: 1475-1487.

609 Brey, S. J., Barnes, E. A., Pierce, J. R., et al. Environmental Conditions, Ignition Type, and Air Quality
610 Impacts of Wildfires in the Southeastern and Western United States. *Earth's Future*[J]: 2018, 6:
611 1442-1456.

612 Cheng, L., McDonald, K. M., Angle, R. P., et al. Forest fire enhanced photochemical air pollution. A case
613 study. *Atmospheric Environment*[J]: 1998, 32: 673-681.

614 Clark, D., Mercado, L., Sitch, S., et al. The Joint UK Land Environment Simulator (JULES), model
615 description—Part 2: carbon fluxes and vegetation dynamics. *Geoscientific Model Development*[J]:
616 2011, 4: 701-722.

617 Curci, G., Beekmann, M., Vautard, R., et al. Modelling study of the impact of isoprene and terpene
618 biogenic emissions on European ozone levels. *Atmospheric Environment*[J]: 2009, 43: 1444-1455.

619 Dang, R. and Liao, H. Severe winter haze days in the Beijing–Tianjin–Hebei region from 1985 to 2017
620 and the roles of anthropogenic emissions and meteorology. *Atmospheric Chemistry and Physics*[J]:
621 2019, 19: 10801-10816.

622 David, L. M., Ravishankara, A., Brewer, J. F., et al. Tropospheric ozone over the Indian subcontinent
623 from 2000 to 2015: Data set and simulation using GEOS-Chem chemical transport model. *Atmospheric*
624 *Environment*[J]: 2019, 219: 117039.

625 Farquhar, G. D., von Caemmerer, S. v. and Berry, J. A. A biochemical model of photosynthetic CO₂
626 assimilation in leaves of C₃ species. *Planta*[J]: 1980, 149: 78-90.

627 Feng, Z. Z., Yuan, X. Y., Fares, S., et al. Isoprene is more affected by climate drivers than monoterpenes:
628 A meta-analytic review on plant isoprenoid emissions. *Plant Cell and Environment*[J]: 2019, 42:
629 1939-1949.

630 Fitzky, A. C., Sandén, H., Karl, T., et al. The interplay between ozone and urban vegetation—BVOC
631 emissions, ozone deposition and tree ecophysiology. *Frontiers in Forests and Global Change*[J]: 2019, 2:
632 50.

633 Fountoukis, C. and Nenes, A. ISORROPIA II: a computationally efficient thermodynamic equilibrium
634 model for K⁺-Ca²⁺-Mg²⁺-NH₄⁺-Na⁺-SO₄²⁻-NO₃⁻-Cl-H₂O aerosols. *Atmospheric Chemistry and Physics*[J]:
635 2007, 7: 4639-4659.

636 Gong, C., Lei, Y., Ma, Y., et al. Ozone-vegetation feedback through dry deposition and isoprene
637 emissions in a global chemistry-carbon-climate model. *Atmospheric Chemistry and Physics*[J]: 2020,
638 20: 3841-3857.

639 Gong, C. and Liao, H. A typical weather pattern for ozone pollution events in North China. *Atmospheric*
640 *Chemistry and Physics*[J]: 2019, 19: 13725-13740.

641 He, C., Clifton, O. and Coauthors. Interactions between Air Pollution and Terrestrial Ecosystems:
642 Perspectives on Challenges and Future Directions. *Bulletin of the American Meteorological Society*[J]:
643 2020, doi: <https://doi.org/10.1175/BAMS-D-20-0066.1>, 2020.

644 Heald, C. L. and Geddes, J. A. The impact of historical land use change from 1850 to 2000 on
645 secondary particulate matter and ozone. *Atmospheric Chemistry and Physics*[J]: 2016, 16:
646 14997-15010.

647 Huntingford, C., Oliver, R. J., Mercado, L. M., et al. Technical note: A simple theoretical model
648 framework to describe plant stomatal “sluggishness” in response to elevated ozone concentrations.

649 Biogeosciences[J]: 2018, 15: 5415-5422.

650 Inada, H., Kondo, T., Akhtar, N., et al. Relationship between cultivar difference in the sensitivity of net
651 photosynthesis to ozone and reactive oxygen species scavenging system in Japanese winter wheat
652 (*Triticum aestivum*). *Physiologia Plantarum*[J]: 2012, 146: 217-227.

653 Jaffe, D. A., Wigder, N., Downey, N., et al. Impact of wildfires on ozone exceptional events in the
654 Western US. *Environ Sci Technol*[J]: 2013, 47: 11065-11072.

655 Jaffe, D. A. and Wigder, N. L. Ozone production from wildfires: A critical review. *Atmospheric*
656 *Environment*[J]: 2012, 51: 1-10.

657 Jiang, X. Y., Wiedinmyer, C. and Carlton, A. G. Aerosols from Fires: An Examination of the Effects on
658 Ozone Photochemistry in the Western United States. *Environmental Science & Technology*[J]: 2012, 46:
659 11878-11886.

660 Juráň, S., Grace, J. and Urban, O. Temporal Changes in Ozone Concentrations and Their Impact on
661 Vegetation. *Atmosphere*[J]: 2021, 12: 82.

662 Karnosky, D. F., Skelly, J. M., Percy, K. E., et al. Perspectives regarding 50 years of research on effects of
663 tropospheric ozone air pollution on US forests. *Environmental Pollution*[J]: 2007, 147: 489-506.

664 Keller, C. A., Long, M. S., Yantosca, R. M., et al. HEMCO v1. 0: a versatile, ESMF-compliant component
665 for calculating emissions in atmospheric models. *Geosci. Model Dev.*[J]: 2014, 7: 1409-1417.

666 Kita, K., Fujiwara, M. and Kawakami, S. Total ozone increase associated with forest fires over the
667 Indonesian region and its relation to the El Nino-Southern oscillation. *Atmospheric Environment*[J]:
668 2000, 34: 2681-2690.

669 Laban, T. L., Van Zyl, P. G., Beukes, J. P., et al. Seasonal influences on surface ozone variability in
670 continental South Africa and implications for air quality. *Atmospheric Chemistry and Physics*[J]: 2018,
671 18: 15491-15514.

672 Lei, Y., Yue, X., Liao, H., et al. Implementation of Yale Interactive terrestrial Biosphere model v1.0 into
673 GEOS-Chem v12.0.0: a tool for biosphere-chemistry interactions. *Geoscientific Model Development*[J]:
674 2020, 13: 1137-1153.

675 Li, S., Chen, L., Huang, G., et al. Retrieval of surface PM_{2.5} mass concentrations over North China using
676 visibility measurements and GEOS-Chem simulations. *Atmospheric Environment*[J]: 2019, 2019.
677 117121.

678 Lombardozi, D., Levis, S., Bonan, G., et al. Predicting photosynthesis and transpiration responses to
679 ozone: decoupling modeled photosynthesis and stomatal conductance. *Biogeosciences*[J]: 2012, 9:
680 3113-3130.

681 Lu, X., Zhang, L., Chen, Y., et al. Exploring 2016-2017 surface ozone pollution over China: source
682 contributions and meteorological influences. *Atmospheric Chemistry and Physics*[J]: 2019, 19:
683 8339-8361.

684 Lu, X., Zhang, L., Yue, X., et al. Wildfire influences on the variability and trend of summer surface
685 ozone in the mountainous western United States. *Atmospheric Chemistry and Physics*[J]: 2016, 16:
686 14687-14702.

687 McLinden, C., Olsen, S., Hannegan, B., et al. Stratospheric ozone in 3 - D models: A simple chemistry
688 and the cross - tropopause flux. *Journal of Geophysical Research: Atmospheres*[J]: 2000, 105:
689 14653-14665.

690 Nuryanto, D. E. Simulation of forest fires smoke using WRF-Chem model with FINN fire emissions in
691 Sumatera. 1st International Symposium on Lapan-Ipb Satellite (Lisat) for Food Security and
692 Environmental Monitoring[J]: 2015, 24: 65-69.

693 Oltmans, S. J., Lefohn, A. S., Harris, J. M., et al. Enhanced ozone over western North America from
694 biomass burning in Eurasia during April 2008 as seen in surface and profile observations. *Atmospheric*
695 *Environment*[J]: 2010, 44: 4497-4509.

696 Pacifico, F., Folberth, G., Sitch, S., et al. Biomass burning related ozone damage on vegetation over the
697 Amazon forest: a model sensitivity study. [J]: 2015, 2015.

698 Paoletti, E., Grulke, N. E. and Matyssek, R. Ozone Amplifies Water Loss from Mature Trees in the Short
699 Term But Decreases It in the Long Term. *Forests*[J]: 2019, 11: 46.

700 Pope, R. J., Arnold, S. R., Chipperfield, M. P., et al. Substantial increases in Eastern Amazon and
701 Cerrado biomass burning-sourced tropospheric ozone. *Geophysical Research Letters*[J]: 2020, 47:
702 e2019GL084143.

703 Sadiq, M., Tai, A. P. K., Lombardozi, D., et al. Effects of ozone-vegetation coupling on surface ozone air
704 quality via biogeochemical and meteorological feedbacks. *Atmospheric Chemistry and Physics*[J]: 2017,
705 17: 3055-3066.

706 Schiferl, L. D. and Heald, C. L. Particulate matter air pollution may offset ozone damage to global crop
707 production. *Atmospheric Chemistry and Physics*[J]: 2018, 18: 5953-5966.

708 Sitch, S., Cox, P. M., Collins, W. J., et al. Indirect radiative forcing of climate change through ozone
709 effects on the land-carbon sink. *Nature*[J]: 2007, 448: 791-794.

710 Spitters, C. Separating the diffuse and direct component of global radiation and its implications for
711 modeling canopy photosynthesis Part II. Calculation of canopy photosynthesis. *Agricultural and Forest*
712 *meteorology*[J]: 1986, 38: 231-242.

713 Travis, K. R., Jacob, D. J., Fisher, J. A., et al. Why do models overestimate surface ozone in the
714 southeastern United States? *Atmospheric Chemistry and Physics*[J]: 2016, 16: 13561.

715 Turetsky, M. R., Kane, E. S., Harden, J. W., et al. Recent acceleration of biomass burning and carbon
716 losses in Alaskan forests and peatlands. *Nature Geoscience*[J]: 2011, 4: 27-31.

717 Val Martin, M., Logan, J. A., Kahn, R. A., et al. Smoke injection heights from fires in North America:
718 analysis of 5 years of satellite observations. *Atmospheric Chemistry and Physics*[J]: 2010, 10:
719 1491-1510.

720 van der Werf, G. R., Randerson, J. T., Giglio, L., et al. Global fire emissions and the contribution of
721 deforestation, savanna, forest, agricultural, and peat fires (1997-2009). *Atmospheric Chemistry and*
722 *Physics*[J]: 2010, 10: 11707-11735.

723 Von Caemmerer, S. v. and Farquhar, G. D. Some relationships between the biochemistry of
724 photosynthesis and the gas exchange of leaves. *Planta*[J]: 1981, 153: 376-387.

725 Vongruang, P., Wongwises, P. and Pimonsree, S. Assessment of fire emission inventories for simulating
726 particulate matter in Upper Southeast Asia using WRF-CMAQ. *Atmospheric Pollution Research*[J]:
727 2017, 8: 921-929.

728 Watson, G. L., Telesca, D., Reid, C. E., et al. Machine learning models accurately predict ozone
729 exposure during wildfire events. *Environmental Pollution*[J]: 2019, 254: 112792.

730 Wiedinmyer, C., Akagi, S. K., Yokelson, R. J., et al. The Fire INventory from NCAR (FINN): a high
731 resolution global model to estimate the emissions from open burning. *Geoscientific Model*
732 *Development*[J]: 2011, 4: 625-641.

733 Wittig, V. E., Ainsworth, E. A., Naidu, S. L., et al. Quantifying the impact of current and future
734 tropospheric ozone on tree biomass, growth, physiology and biochemistry: a quantitative
735 meta-analysis. *Global Change Biology*[J]: 2009, 15: 396-424.

736 Yan, Y., Lin, J. and He, C. Ozone trends over the United States at different times of day. *Atmospheric*

737 Chemistry and Physics[J]: 2018, 18: 1185.
738 Yue, X., Keenan, T. F., Munger, W., et al. Limited effect of ozone reductions on the 20-year
739 photosynthesis trend at Harvard forest. Global Change Biology[J]: 2016, 22: 3750-3759.
740 Yue, X., Mickley, L., Logan, J., et al. Impact of 2050 climate change on North American wildfire:
741 consequences for ozone air quality. Atmospheric Chemistry and Physics[J]: 2015, 15: 10033-10055.
742 Yue, X. and Unger, N. Ozone vegetation damage effects on gross primary productivity in the United
743 States. Atmospheric Chemistry and Physics[J]: 2014, 14: 9137-9153.
744 Yue, X. and Unger, N. The Yale Interactive terrestrial Biosphere model version 1.0: description,
745 evaluation and implementation into NASA GISS ModelE2. Geoscientific Model Development[J]: 2015,
746 8: 2399-2417.
747 Yue, X. and Unger, N. Fire air pollution reduces global terrestrial productivity. Nat Commun[J]: 2018, 9:
748 5413.
749 Zhang, L., Jacob, D. J., Downey, N. V., et al. Improved estimate of the policy-relevant background ozone
750 in the United States using the GEOS-Chem global model with 1/2x2/3 horizontal resolution over North
751 America. Atmospheric Environment[J]: 2011, 45: 6769-6776.
752 Zhou, S. S., Tai, A. P. K., Sun, S. H., et al. Coupling between surface ozone and leaf area index in a
753 chemical transport model: strength of feedback and implications for ozone air quality and vegetation
754 health. Atmospheric Chemistry and Physics[J]: 2018, 18: 14133-14148.
755 Zhu, J., Tai, A. P. K. and Yim, S. H. L. Effects of ozone-vegetation interactions on meteorology and air
756 quality in China using a two-way coupled land-atmosphere model. Atmos. Chem. Phys. Discuss.
757 [preprint][J]: 2021, doi: <https://doi.org/10.5194/acp-2021-165>, 2021.
758 Ziemke, J. R., Chandra, S., Duncan, B. N., et al. Recent biomass burning in the tropics and related
759 changes in tropospheric ozone. Geophysical Research Letters[J]: 2009, 36: L15819.
760
761
762
763
764
765

Formatted: Indent: Left: 0 cm, Hanging: 2 ch, First line: -2 ch

766

767 **Table 1** Summary of simulations using the GC-YIBs model

Name	Emissions	O ₃ damaging	O ₃ sensitivities
CTRL_FIRE_HS	All including fires	Offline	High
CTRL_FIRE_LS	All including fires	Offline	Low
CTRL_NOFIRE_HS	All but without fires	Offline	High
CTRL_NOFIRE_LS	All but without fires	Offline	Low
O3CPL_FIRE_HS	All including fires	Online	High
O3CPL_FIRE_LS	All including fires	Online	Low
O3CPL_NOFIRE_HS	All but without fires	Online	High
O3CPL_NOFIRE_LS	All but without fires	Online	Low

768

769

770

771

772

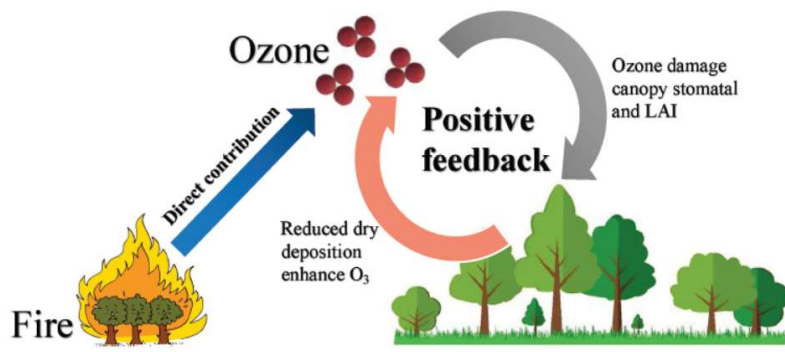
773

774

775

776

777



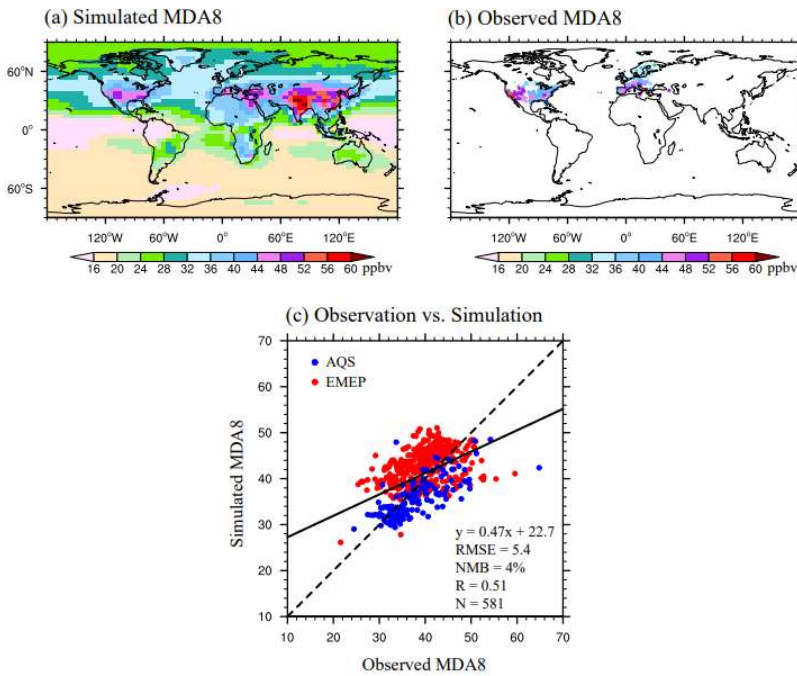
778

779 **Figure 1** Diagram of the impacts of fires on surface O₃ through direct emissions and

780 O₃-vegetation feedback.

781

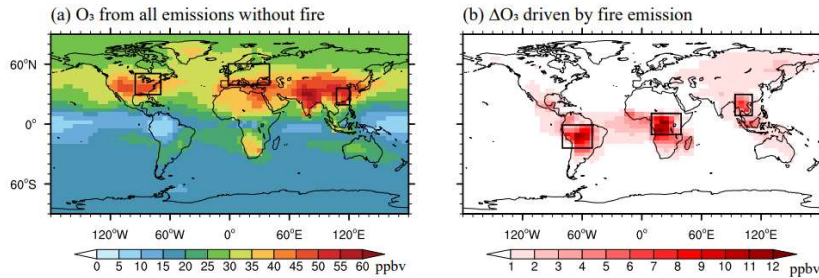
782



783
784

785 **Figure 2** Spatial pattern of (a) simulated and (b) observed surface $[O_3]$. (c) Scatter
 786 plot of surface $[O_3]$ over measurements in two regions. The black line shows the
 787 linear regression between the observed and simulated $[O_3]$. The regression fit,
 788 correlation coefficient (R), root mean square error (RMSE), and normalized mean bias
 789 (NMB) are shown in the bottom panel with an indication of site numbers (N) used for
 790 statistics.

791



792

793 **Figure 3** Annual surface [O₃] from (a) nonfire and (b) fire-alone sources. The six
 794 subregions are marked with black boxes: Eastern U.S. (EUS, 30°N-50°N,
 795 95°W-70°W), Western Europe (WEU, 40°N-60°N, 0°-40°E), Eastern China (ECH,
 796 20°N-35°N, 108°E-120°E), Amazon (AMZ, 25°S-0°, 80°W-50°W), Central Africa
 797 (CAF, 10°S-10°N, 10°E-40°E), and Southern Asia (SAS, 10°N-30°N, 95°E-110°E).

798

799

800

801

802

803

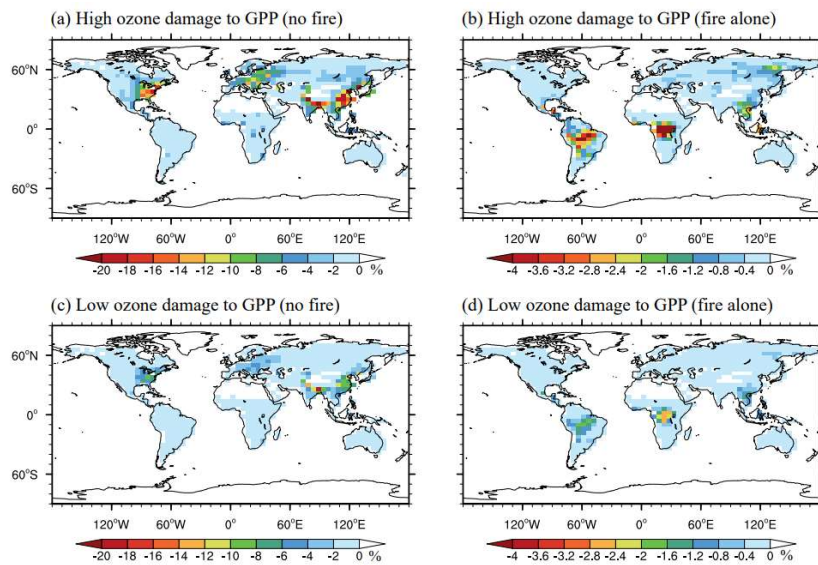
804

805

806

807

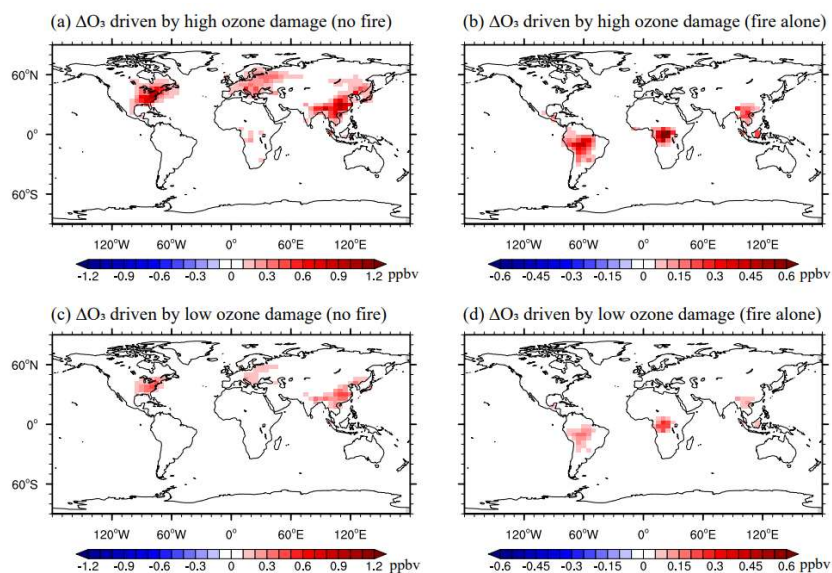
808



809

810 **Figure 4** Annual percentage of reductions in GPP caused by O₃ from (a, c) nonfire
 811 and (b, d) fire alone sources with (a, b) high and (c, d) low O₃ sensitivities. Please
 812 note the differences in color scales.

813



814

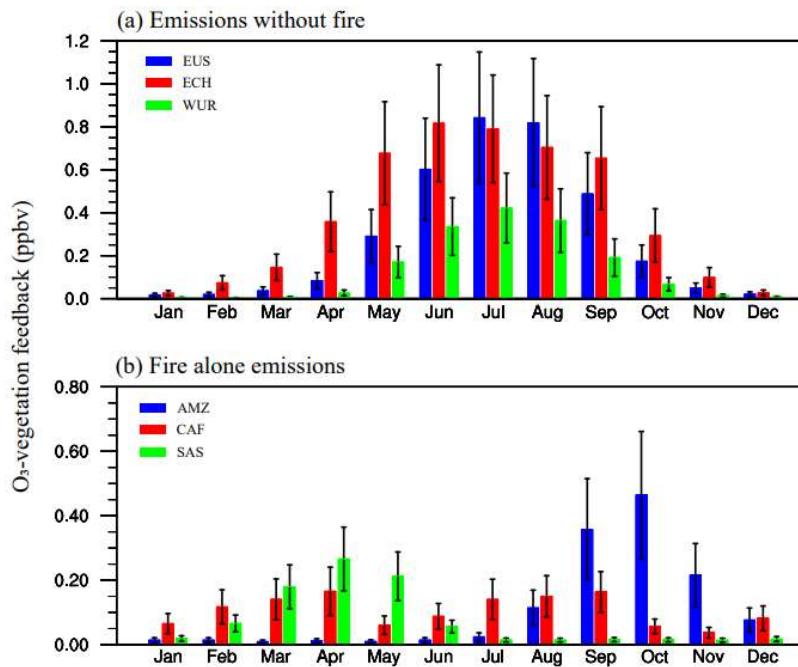
815 **Figure 5** Annual feedback to surface O_3 caused by O_3 vegetation damage with (a, b)

816 high and (c, d) low O_3 sensitivities. (a) and (c) represent feedback by O_3 from nonfire

817 sources; (b) and (d) represent feedback by O_3 from fire emissions alone. Please note

818 the differences in color scales.

819



820

821 **Figure 6** Seasonal variations in O₃-vegetation feedback driven by (a) nonfire and (b)
 822 fire-alone sources. The blue, red, and green bars in (a) represent the O₃-vegetation
 823 feedback in Eastern U.S. (EUS), Eastern China (ECH), Western Europe (WUR),
 824 respectively. The blue, red, and green bars in (b) represent the O₃-vegetation feedback
 825 in Amazon (AMZ), Central Africa (CAF), and Southern Asia (SAS), respectively. The
 826 error bars represent low to high O₃ damaging sensitivities.

827

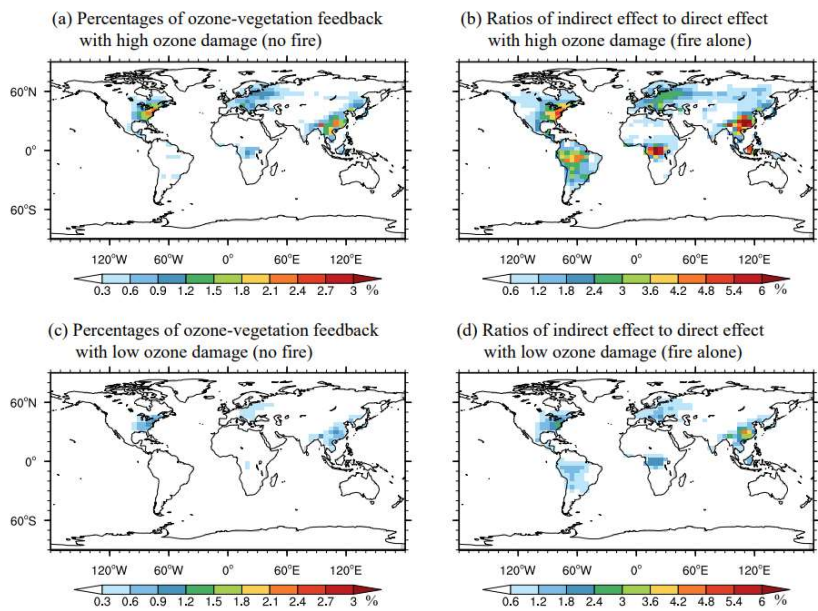
828

829

830

831

Deleted: ¶
¶
¶
¶



836

837 **Figure 7** Annal ratios of indirect $\Delta[\text{O}_3]$ to ambient $[\text{O}_3]$ from (a, c) nonfire emissions
 838 and the ratios of indirect to direct $\Delta[\text{O}_3]$ from (b, d) fire emissions alone with (a, b)
 839 high and (c, d) low O_3 damaging sensitivities. Please note the differences in color
 840 scales.

841

842